Control of Electron Wave Packets Close to the Continuum Threshold Using Near-Single-Cycle THz Waveforms

Simon Brennecke,[1] Martin Ranke,[2,3] Anastasios Dimitriou,[2,3,4] Sophie Walther,[2,3] Mark J. Prandolini,[2] Manfred Lein,[1,*] and Ulrike Frühling[2,3,5,†]

[1]*Leibniz Universität Hannover, Institut für Theoretische Physik, Appelstraße 2, 30167 Hannover, Germany*
[2]*Institut für Experimentalphysik, Universität Hamburg, Luruper Chaussee 149, 22761 Hamburg, Germany*
[3]*The Hamburg Centre for Ultrafast Imaging (CUI), Luruper Chaussee 149, 22761 Hamburg, Germany*
[4]*Institute of Nanoscience and Nanotechnology, NCSR Demokritos, 15341 Agia Paraskevi, Athens, Greece*
[5]*Deutsches Elektronen-Synchrotron, Notkestrasse 85, 22603 Hamburg, Germany*

(Received 29 April 2022; accepted 17 October 2022; published 18 November 2022; corrected 29 December 2022)

The control of low-energy electrons by carrier-envelope-phase-stable near-single-cycle THz pulses is demonstrated. A femtosecond laser pulse is used to create a temporally localized wave packet through multiphoton absorption at a well defined phase of a synchronized THz field. By recording the photoelectron momentum distributions as a function of the time delay, we observe signatures of various regimes of dynamics, ranging from recollision-free acceleration to coherent electron-ion scattering induced by the THz field. The measurements are confirmed by three-dimensional time-dependent Schrödinger equation simulations. A classical trajectory model allows us to identify scattering phenomena analogous to strong-field photoelectron holography and high-order above-threshold ionization.

DOI: 10.1103/PhysRevLett.129.213202

The light-based control of electrons forms the foundation of ultrafast science and enables the observation of quantum dynamics on its inherent time and length scale [1–4]. In many of the ultrafast methods, laser-induced tunneling creates an electron wave packet in the continuum, which is afterwards controlled by the same laser field and potentially driven back to the parent ion, resulting in a head-on collision of a high-energy electron [5]. Recollisions lead to important phenomena such as high-harmonic generation [6], elastic scattering and diffraction [7,8], or photoelectron holography [9]. However, when considering electrons with low energies close to the continuum threshold, the long-range Coulomb force acting between the electron and the parent ion becomes more important. Just above the continuum threshold, the photoelectron spectra from atoms in strong laser pulses show "low-energy structures" [10–13] caused by soft recollisions in the Coulomb field [12–16]. Just below the continuum threshold, a quasicontinuum of Rydberg states can be populated through multiphoton absorption [17–20] or by recapture after tunnel ionization [21–25]. The excited states play an important role in the generation of coherent vacuum-ultraviolet (VUV) emission [26–29].

A major obstacle in controlling electron wave packets with a single pulse is that both the creation of the wave packet and its further motion are governed by the same field. In this Letter, we implement the natural solution by using two light fields such that each field is responsible for only one of the two steps. Multiphoton ionization by a short near-infrared (NIR) pulse with 25 fs duration creates an electron wave packet at the continuum edge, i.e., extending across weakly bound and continuum states. Afterwards the motion of the wave packet is controlled by a carrier-envelope-phase-stable near-single-cycle THz pulse with a cycle length of about 1.3 ps at the central frequency. Hence, the launch time of the wave packet is localized on the scale of an optical cycle of the THz field. This subcycle timing allows us to control what physical processes take place, ranging from weak Coulomb focusing of the outgoing wave packet over pronounced collision dynamics, such as large-angle scattering and the appearance of caustics, to chaotic ionization of Rydberg states. Pump-probe schemes based on the ionization with THz pulses [30,31] have been implemented previously to study the dynamics of weakly bound states [32,33] and to control the recombination of low-energy continuum electrons on a picosecond timescale [34]. By employing a combination with a short NIR pulse, our setup offers—compared to earlier work—a high time resolution of the THz induced near-threshold processes. It gives detailed insight into the dynamics by measuring photoelectron momentum distributions (PMDs) by velocity-map imaging [35,36].

Our setup is comparable to the attosecond streak camera where an extreme ultraviolet attosecond pulse creates a temporally localized electron wave packet by single-photon ionization and afterwards the photoelectrons are streaked in energy by means of a femtosecond infrared laser pulse [37–39]. At low electron energies (in the few-eV range), theoretical work has shown that streaking may involve recollision-induced scattering phenomena [40–45]. A similar method, using an attosecond pulse train phase-locked to

the infrared field [46], has already been used in experiments to manipulate and probe electron wave packets at low energies [47–50]. Depending on the delay between the pulse train and the infrared field, recollisions have been observed in photoelectron distributions [51] and in the emitted radiation [52,53]. The series of wave packets created by the pulse train makes the analysis more challenging. We note also that in these studies the degree of temporal localization of the initial wave packet, quantified as the ratio of probe cycle length to ionizing pulse length, is around 10, i.e., much lower than in the present THz-NIR scheme with a ratio of about 50.

In our experiment, a linearly polarized NIR beam from a Ti:sapphire laser centered at 795 nm wavelength (photon energy $\omega \approx 1.56$ eV) with a pulse duration of ≈25 fs (FWHM) and a pulse energy of 3 mJ at 1 kHz repetition rate is split into two parts. One part is sent to a delay stage and afterwards used to generate THz pulses by optical rectification in a 0.6% MgO-doped congruent $LiNbO_3$ crystal, employing the tilted-pulse-front method [54,55]. The THz output is focused using an off-axis parabolic mirror (OAPM) with a focal length of 101.6 mm. The remaining NIR laser beam is focused by a spherical mirror with a focal length of 500 mm and directed through a 2 mm central aperture in the OAPM, whereby it is collinearly superimposed with the THz beam. The THz pulses are near-single-cycle pulses with a central frequency of 0.78 THz. A large THz focus radius of 1.1 mm ensures a spatially homogeneous THz field in the relevant reaction volume. A home-built velocity-map imaging spectrometer (VMI) is used to measure the 2D projections of the PMDs of outgoing electrons [35,36,56]. In the VMI, xenon atoms are supplied by a high-resistance lead-glass capillary. The static electric field of the VMI in the interaction region is 20.5 kV/m. The polarization of the light pulses (x axis) is parallel to the detector plane, see the illustration in Fig. 1(a). The time delay between NIR and THz pulses is varied in steps of ≈29 fs, and each distribution is averaged over 2500 shots.

For a theoretical description, we solve the time-dependent Schrödinger equation (TDSE) numerically in the single-active-electron approximation using a modified Green-Sellin-Zachor potential for xenon, reproducing the ionization potential of $I_p \approx 0.4458$ a.u. (for $^2P_{3/2}$ ionic states) [57–59]. The THz waveform and a NIR pulse with a $\sin^2$ envelope of 26 cycles duration and $I = 7 \times 10^{12}$ W/cm^2 intensity are taken into account in the simulation. The numerical propagation uses the pseudospectral method in length gauge [60,61]. The angular dependence of the wave function is expanded in spherical harmonics with maximal orbital angular momentum $l_{\max} = 512$. The radial part is discretized on a nonuniform grid extending to $r_{\max} = 19\,000$ a.u. such that it covers the low-energy part of the wave function until the end of the THz pulse. To calculate accurate PMDs, we project the final wave function onto scattering states for the ionic potential.

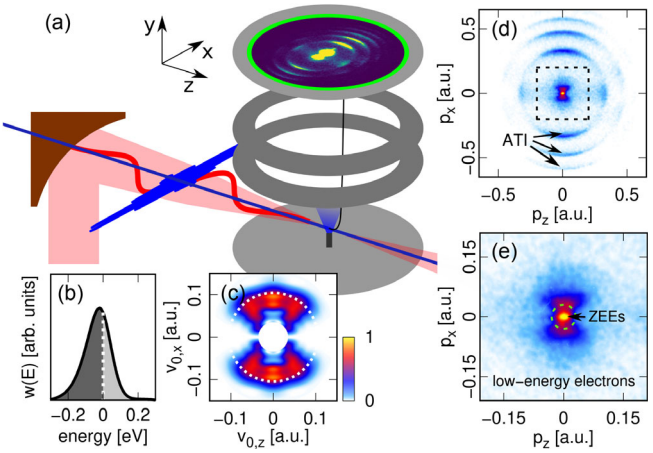

FIG. 1. (a) Sketch of the experimental setup. A NIR pulse creates an electron wave packet at the continuum edge in xenon and a time-delayed THz waveform is used to control the dynamics. (b) Energy distribution from the TDSE simulation without THz pulse. (c) Simulated wave packet still localized close to the ionic core at the end of the NIR pulse and here represented by a slice through its velocity distribution. The white dotted lines indicate zero energy, see text. (d) Measured projection of the full PMD without THz pulse and (e) magnification of the low-energy region.

We first study the PMD without the THz waveform. In a multiphoton picture, a photon number of $N = 9$ is at least required to overcome the ionization potential I_p of xenon as well as the ponderomotive potential $U_p \propto I/\omega^2$ and to form above-threshold-ionization (ATI) peaks [62], see the measured projection of the PMD in Fig. 1(d). However, since the estimated intensity 7×10^{12} W/cm^2 is just above the closing of an ionization channel (occurring when $N\omega - I_p - U_p \approx 0$), an eight-photon peak appears slightly below the continuum threshold, see the calculated energy distribution in Fig. 1(b). In the low-energy part of the measured PMD, presented in Fig. 1(e), the positive-energy tail of this peak results in an extended "butterfly-shaped" pattern. Additionally, a bright spot of "zero-energy electrons" (ZEEs) centered at $p = 0$ is visible. It is attributed to ionization of Rydberg states after the NIR pulse by the VMI extraction field [63,64] or by blackbody radiation [65].

The THz pulse modifies the dynamics of the wave packet. For electrons with sufficiently high energy, the influence of the Coulomb field can be neglected and the same basic concept as in the attosecond streak camera [38,66,67] holds: the momentum change of electrons induced by the THz field can be classically approximated as $\Delta p_x = -\int_\tau^\infty E_{\mathrm{THz}}(t)dt = -A_{\mathrm{THz}}(\tau)$, where τ is the creation time (equal to the delay). E_{THz} and A_{THz} are the electric field and the vector potential of the THz waveform, respectively. The experimental THz pulse is reconstructed from streaking of the nine-photon ATI peak (at ≈1.5 eV);

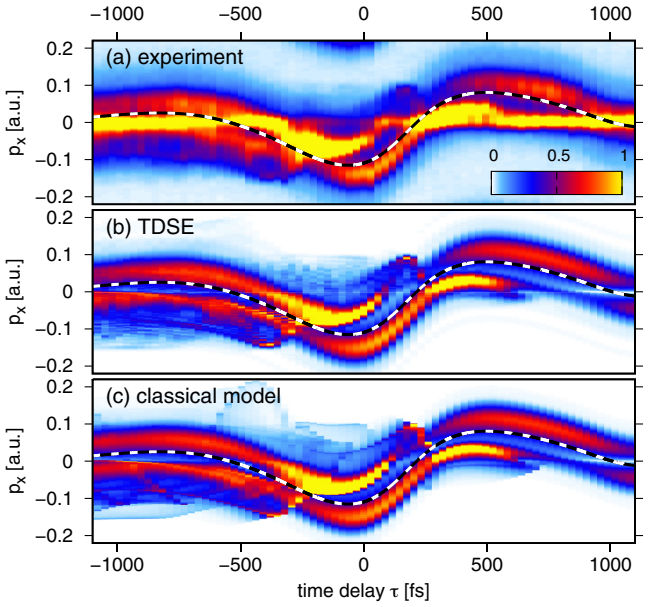

FIG. 2. Electron momentum distribution along the polarization direction (p_x direction) versus time delay between the THz waveform and the NIR pulse: (a) experiment, (b) TDSE, (c) classical model. The distributions are obtained by integration of the 2D projections over $|p_z| < 0.1$ a.u. The dashed line shows the momentum shift $\Delta p_x = -A_{\mathrm{THz}}(\tau)$, i.e., estimated by neglecting the electron-core interaction.

the negative THz vector potential is shown in Fig. 2 as a dashed line. Although the maximal THz field strength is only about 81 kV/cm $\approx 1.58 \times 10^{-5}$ a.u., the long acceleration time of the THz field leads to momentum changes on the order of 0.1 a.u.

In contrast to the well-established high-energy streaking, we observe major deviations from such a simple momentum shift at low energies. Figure 2 shows the momentum distributions along the polarization axis for low-energy electrons as a function of the delay. The complete 2D projections of the PMDs are available as Supplemental Material [68]. Although the momentum distributions follow roughly the estimated momentum shift, they are strongly deformed and show a modulation of the total probability. In addition, unexpected structures appear, e.g., at $p_x \approx 0.09$ a.u. for the delay $\tau \approx 174$ fs. Furthermore, the p_x distributions are noticeably broader when the wave packet is created before the main THz pulse arrives (large negative delays) compared to creation after the main THz pulse has already passed (large positive delays). Except for the ZEEs appearing at $p_x = 0$ in the measurement, all major features are well reproduced by the TDSE simulation. The enhancement of ZEEs is mainly due to the detector field, see Supplemental Material [68].

To reveal the underlying physics, we use a classical trajectory-based model. The initial wave packet created at a time τ by the NIR field is calculated from a numerical simulation of the TDSE without THz field. To represent the wave packet by a classical phase-space distribution, we use the velocity distribution, shown in Fig. 1(c), and assign to each velocity $\mathbf{v}_0$ a unique initial position $\mathbf{r}_0(\mathbf{v}_0) = r_0(v_0)\hat{\mathbf{v}}_0$. The mapping $r_0(v_0)$ is optimized to reproduce the THz-field-free energy distribution, resulting in initial positions between ≈100 a.u. and ≈200 a.u. By construction, this model assigns a unique energy value to each initial velocity and thus allows us to identify regions of negative and positive energies, see the white dotted line in Fig. 1(c). Without the THz field, the wave packet moves outwards and is only slowed down by the long-range Coulomb force. Electrons with negative energies reach their classical turning points and stay trapped, resulting in excited atoms. Electrons with positive energies escape and form the THz-field-free PMD. Additional dynamics is induced by the THz pulse. We treat this motion by propagating a swarm of trajectories following Newton's equation in the presence of the THz field and a $-1/r$ Coulomb potential. The classical model reproduces well the major features of the TDSE distributions, see Fig. 2(c).

For a wave packet created close to a zero crossing of the THz electric field, e.g., at −58 fs delay, the first half-cycle of the remaining THz pulse accelerates the parts with negative $v_{0,x}$ components further; see the trajectory drawn as a black dotted line in Fig. 3(e). Analogous to streaking of high-energy electrons, these parts do not revisit the ionic core and are only decelerated by the ionic potential. For −58 fs delay, this leads to the trianglelike region at $p_x <$ −0.1 a.u. in the projected PMDs shown in Figs. 3(a) and 3(c). Classically, both negative and positive initial energies E_0 contribute to this region. In Fig. 3(c), $E_0 = 0$ is indicated as a white dotted line. The angular structure of the initial velocity distribution leaves an imprint on the shape of this structure. Thus, information not only on the energy distribution of Rydberg states but also on their initial wave-packet shape is encoded in the projected PMDs.

On the other hand, trajectories starting initially with $v_{0,x}$ components parallel to the THz field are first decelerated by the THz field and may reverse their direction. If their lateral velocity is large, the trajectories are still only weakly influenced by the Coulomb field as shown by the blue dashed-dotted trajectory in Fig. 3(e). However, for smaller lateral velocities, the electrons may be driven back to the vicinity of the parent ion and scatter off; see the blue and red solid trajectories in Fig. 3(e). Thus, different parts of the wave packet are deflected to the same final momenta. For example, the blue dotted, dashed-dotted, and solid trajectories contribute to region B of the distribution for −58 fs delay. This situation is similar to strong-field photoelectron holography [9,69] and, hence, close inspection shows an interference pattern in the TDSE simulations, which is, however, not resolved in the experiment. The scattering angles of the electrons increase for smaller initial lateral velocities, leading to larger final lateral momenta, see region C in Figs. 3(a) and 3(c). Thus, analogous to

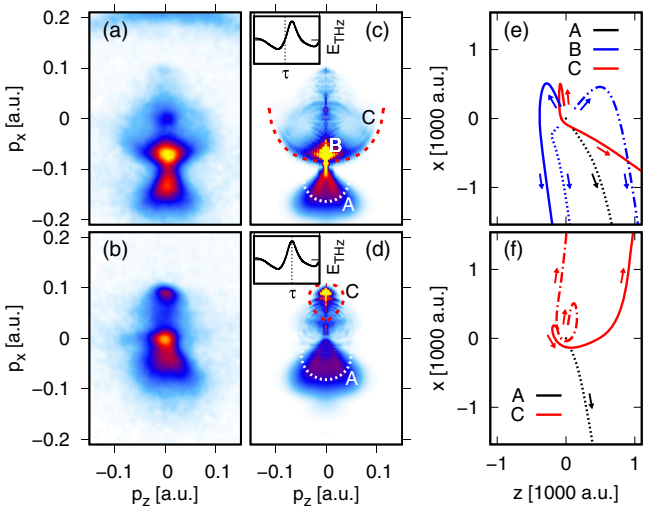

FIG. 3. 2D projections of the PMDs for −58 fs delay (upper panels) and 174 fs delay (lower panels): experimental results [(a), (b)] and TDSE results [(c),(d)]. The white dotted lines indicate zero initial energy and the red dashed lines mark the classical boundary of the scattering plateau. The electric field E_{THz} is shown in the insets. Characteristic trajectories corresponding to the regions marked in panels (c) and (d) are depicted in panels (e) and (f).

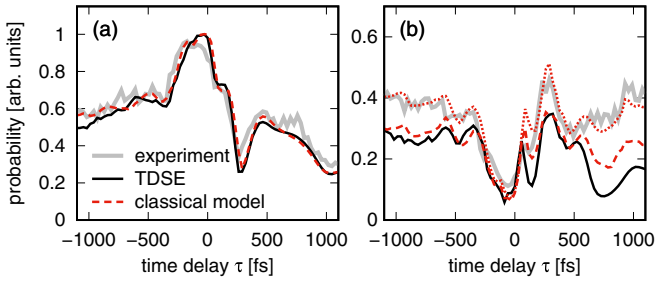

FIG. 4. Integrated probabilities versus time delay. (a) Low-energy electrons except for ZEEs, obtained by integration over all momenta satisfying $|p_x + A_x(\tau)| < 0.2$ a.u., $|p_z| < 0.1$ a.u. and $\sqrt{p_x^2 + p_z^2} > 0.04$ a.u.: arbitrarily normalized measurement (gray thick lines), TDSE results for a short THz pulse (black lines), and classical model for a THz pulse with tail (red dashed lines). Simulation results are normalized to maximum value 1. (b) Probability of ZEEs ($\sqrt{p_x^2 + p_z^2} < 0.04$ a.u.). The dotted line shows the sum of the classical result and a selected amount of electrons freed by the detector field.

high-order above-threshold ionization [7,8], a circular plateau structure is formed. Its classical boundary is indicated in Fig. 3(c) as a red dashed line.

For slightly earlier or later delays, the overall shape of the distributions remains unchanged and only the positions and sizes of the various structures are altered. For example, the extension of the plateau shrinks for later delays and, thus, a large region of initial velocities is mapped to a tiny region in final momentum space. In the classical simulations, this bunching of the electron trajectories causes a caustic at ≈174 fs delay, corresponding to a bright spot at $p_x \approx 0.09$ a.u. in the experimental and TDSE results shown in Figs. 3(b) and 3(d). For even later delays, after the maximum of the THz electric field, the THz field is not able to guide electrons with velocity components $v_{0,x} > 0$ efficiently back to the core. Hence, the dynamics and the resulting visible structures are substantially altered. Despite the shortness of our near-single-cycle THz pulse, half an optical cycle earlier or later, similar PMD structures can be observed in the reversed direction.

When considering very early delays, the electrons experience the whole THz pulse. In this limit, the continuum part of the wave packet has already traveled far away from the core, when the main part of the THz pulse arrives. Hence, it is only weakly influenced by the THz pulse. In contrast, most bound parts have reached their classical turning points and the bound wave packet is dispersed. When these weakly bound electrons are ionized by the THz pulse like in the earlier works [31,70], then the interplay between the THz pulse and the ionic potential results in a complex chaotic classical motion with multiple revisits to the core. This causes various additional structures visible in the calculated PMDs, see Figs. 2(b) and 2(c). In the experiment, these structures are not fully resolved and they appear as a blurred signal at -0.15 a.u. $\lesssim p_x \lesssim 0.1$ a.u., see Fig. 2(a).

Figure 4(a) displays the low-energy electrons' yield (except for ZEEs) as a function of the delay, showing good agreement between experiment and TDSE. In contrast, the intensity modulation of the ZEEs visible in Fig. 2(a) is not well reproduced by our TDSE simulations, see Fig. 4(b). So far, we only considered a near-single-cycle THz pulse with vanishing field strength outside the pulse length of 2.9 ps. However, the experimental THz waveform has a weak, but long tail [67]. Including a pulse tail in the classical simulations, we observe additional emission of ZEEs and, more importantly, excitation within bound states. The VMI extraction field afterwards depletes these weakly bound states and modifies the dynamics of ZEEs [71], see Supplemental Material [68]. For a simple model, we assume above-barrier ionization by the detector field F such that two-thirds of the bound electrons with energies $|E| < 2\sqrt{F} \approx 11$ meV are freed [72,73]. The result is shown as a red dotted line in Fig. 4(b). Despite its simplicity, the model reproduces well the variation of ZEEs. For example, for delays between −250 fs and 0 fs, the main part of the THz pulse already depletes the weakly bound states and accelerates these electrons, resulting in few ZEEs.

In conclusion, we have demonstrated the control of electron wave packets at the continuum threshold by near-single-cycle THz pulses. The wave-packet creation by a short femtosecond pulse at a defined THz phase provides access to various regimes of dynamics. In the case of recollision-free motion, the measured PMDs contain information on the initial wave packet. In the future, this

imaging capability could be exploited, e.g., to study trapping in Rydberg states after strong-field ionization [19,21] or in two-color fields [74,75]. We have also shown that electrons can be guided back to their parent ions by the THz field, resulting in scattering phenomena reminiscent of well-known strong-field processes. Transferring the related techniques from attosecond physics to the motion of low-energy electrons with their longer time scale and larger length scale can pave the way to the investigation of so far unexplored dynamics in molecules [23,76] or involving multiple electrons [77]. For example, the THz period is comparable to the time scale of dissociation of rare gas dimers in [23] where recapture of multiple electrons was observed, so a THz field could be used to manipulate the number of recaptured electrons and the site of recombination.

This work has been financially supported by the Deutsche Forschungsgemeinschaft through the excellence cluster The Hamburg Centre for Ultrafast Imaging: Structure, Dynamics and Control of Matter at the Atomic Scale—EXC1074 project ID 194651731. S. W. acknowledges financial support from the DFG Forschergruppe FOR 1789. M. L. has been supported by the Deutsche Forschungsgemeinschaft through the Priority Programme Quantum Dynamics in Tailored Intense Fields (QUTIF). We thank N. Kabachnik for helpful discussions.

S. B. and M. R. contributed equally to this work.

*lein@itp.uni-hannover.de
†ulrike.fruehling@desy.de

[1] P. B. Corkum and F. Krausz, Attosecond science, Nat. Phys. **3**, 381 (2007).
[2] F. Krausz and M. Ivanov, Attosecond physics, Rev. Mod. Phys. **81**, 163 (2009).
[3] F. Calegari, G. Sansone, S. Stagira, C. Vozzi, and M. Nisoli, Advances in attosecond science, J. Phys. B **49**, 062001 (2016).
[4] P. Peng, C. Marceau, and D. M. Villeneuve, Attosecond imaging of molecules using high harmonic spectroscopy, Nat. Rev. Phys. **1**, 144 (2019).
[5] P. B. Corkum, Plasma Perspective on Strong Field Multiphoton Ionization, Phys. Rev. Lett. **71**, 1994 (1993).
[6] A. McPherson, G. Gibson, H. Jara, U. Johann, T. S. Luk, I. A. McIntyre, K. Boyer, and C. K. Rhodes, Studies of multiphoton production of vacuum-ultraviolet radiation in the rare gases, J. Opt. Soc. Am. B **4**, 595 (1987).
[7] G. G. Paulus, W. Nicklich, H. Xu, P. Lambropoulos, and H. Walther, Plateau in Above Threshold Ionization Spectra, Phys. Rev. Lett. **72**, 2851 (1994).
[8] D. Ray, B. Ulrich, I. Bocharova, C. Maharjan, P. Ranitovic, B. Gramkow, M. Magrakvelidze, S. De, I. V. Litvinyuk, A. T. Le, T. Morishita, C. D. Lin, G. G. Paulus, and C. L. Cocke, Large-Angle Electron Diffraction Structure in Laser-Induced Rescattering from Rare Gases, Phys. Rev. Lett. **100**, 143002 (2008).
[9] Y. Huismans *et al.*, Time-resolved holography with photoelectrons, Science **331**, 61 (2011).
[10] R. Moshammer, J. Ullrich, B. Feuerstein, D. Fischer, A. Dorn, C. D. Schröter, J. R. Crespo Lopez-Urrutia, C. Hoehr, H. Rottke, C. Trump, M. Wittmann, G. Korn, and W. Sandner, Rescattering of Ultralow-Energy Electrons for Single Ionization of Ne in the Tunneling Regime, Phys. Rev. Lett. **91**, 113002 (2003).
[11] C. I. Blaga, F. Catoire, P. Colosimo, G. G. Paulus, H. G. Muller, P. Agostini, and L. F. DiMauro, Strong-field photoionization revisited, Nat. Phys. **5**, 335 (2009).
[12] W. Quan, Z. Lin, M. Wu, H. Kang, H. Liu, X. Liu, J. Chen, J. Liu, X. T. He, S. G. Chen, H. Xiong, L. Guo, H. Xu, Y. Fu, Y. Cheng, and Z. Z. Xu, Classical Aspects in Above-Threshold Ionization with a Midinfrared Strong Laser Field, Phys. Rev. Lett. **103**, 093001 (2009).
[13] C. Y. Wu, Y. D. Yang, Y. Q. Liu, Q. H. Gong, M. Y. Wu, X. Liu, X. L. Hao, W. D. Li, X. T. He, and J. Chen, Characteristic Spectrum of Very Low-Energy Photoelectron from Above-Threshold Ionization in the Tunneling Regime, Phys. Rev. Lett. **109**, 043001 (2012).
[14] T.-M. Yan, S. V. Popruzhenko, M. J. J. Vrakking, and D. Bauer, Low-Energy Structures in Strong Field Ionization Revealed by Quantum Orbits, Phys. Rev. Lett. **105**, 253002 (2010).
[15] C. Liu and K. Z. Hatsagortsyan, Origin of Unexpected Low Energy Structure in Photoelectron Spectra Induced by Midinfrared Strong Laser Fields, Phys. Rev. Lett. **105**, 113003 (2010).
[16] A. Kästner, U. Saalmann, and J. M. Rost, Electron-Energy Bunching in Laser-Driven Soft Recollisions, Phys. Rev. Lett. **108**, 033201 (2012).
[17] M. P. de Boer and H. G. Muller, Observation of Large Populations in Excited States After Short-Pulse Multiphoton Ionization, Phys. Rev. Lett. **68**, 2747 (1992).
[18] R. R. Jones, D. W. Schumacher, and P. H. Bucksbaum, Population trapping in Kr and Xe in intense laser fields, Phys. Rev. A **47**, R49 (1993).
[19] H. Zimmermann, S. Patchkovskii, M. Ivanov, and U. Eichmann, Unified Time and Frequency Picture of Ultrafast Atomic Excitation in Strong Laser Fields, Phys. Rev. Lett. **118**, 013003 (2017).
[20] Y. Mi, N. Camus, L. Fechner, M. Laux, R. Moshammer, and T. Pfeifer, Electron-Nuclear Coupling through Autoionizing States after Strong-Field Excitation of H_2 Molecules, Phys. Rev. Lett. **118**, 183201 (2017).
[21] T. Nubbemeyer, K. Gorling, A. Saenz, U. Eichmann, and W. Sandner, Strong-Field Tunneling without Ionization, Phys. Rev. Lett. **101**, 233001 (2008).
[22] N. I. Shvetsov-Shilovski, S. P. Goreslavski, S. V. Popruzhenko, and W. Becker, Capture into Rydberg states and momentum distributions of ionized electrons, Laser Phys. **19**, 1550 (2009).
[23] J. Wu, A. Vredenborg, B. Ulrich, L. Ph. H. Schmidt, M. Meckel, S. Voss, H. Sann, H. Kim, T. Jahnke, and R. Dörner, Multiple Recapture of Electrons in Multiple Ionization of the Argon Dimer by a Strong Laser Field, Phys. Rev. Lett. **107**, 043003 (2011).

[24] A. Emmanouilidou, C. Lazarou, A. Staudte, and U. Eichmann, Routes to formation of highly excited neutral atoms in the breakup of strongly driven H_2, Phys. Rev. A **85**, 011402(R) (2012).
[25] S. P. Xu, M. Q. Liu, S. L. Hu, Z. Shu, W. Quan, Z. L. Xiao, Y. Zhou, M. Z. Wei, M. Zhao, R. P. Sun, Y. L. Wang, L. Q. Hua, C. Gong, X. Y. Lai, J. Chen, and X. J. Liu, Observation of a transition in the dynamics of strong-field atomic excitation, Phys. Rev. A **102**, 043104 (2020).
[26] J. Henkel, T. Witting, D. Fabris, M. Lein, P. L. Knight, J. W. G. Tisch, and J. P. Marangos, Prediction of attosecond light pulses in the VUV range in a high-order-harmonic-generation regime, Phys. Rev. A **87**, 043818 (2013).
[27] M. Chini, X. Wang, Y. Cheng, H. Wang, Y. Wu, E. Cunningham, P.-C. Li, J. Heslar, D. A. Telnov, S.-I. Chu, and Z. Chang, Coherent phase-matched VUV generation by field-controlled bound states, Nat. Photonics **8**, 437 (2014).
[28] S. Beaulieu, S. Camp, D. Descamps, A. Comby, V. Wanie, S. Petit, F. Légaré, K. J. Schafer, M. B. Gaarde, F. Catoire, and Y. Mairesse, Role of Excited States in High-Order Harmonic Generation, Phys. Rev. Lett. **117**, 203001 (2016).
[29] H. Yun, J. H. Mun, S. I. Hwang, S. B. Park, I. A. Ivanov, C. H. Nam, and K. T. Kim, Coherent extreme-ultraviolet emission generated through frustrated tunnelling ionization, Nat. Photonics **12**, 620 (2018).
[30] R. R. Jones, D. You, and P. H. Bucksbaum, Ionization of Rydberg Atoms by Subpicosecond Half-Cycle Electromagnetic Pulses, Phys. Rev. Lett. **70**, 1236 (1993).
[31] S. Li and R. R. Jones, Ionization of Excited Atoms by Intense Single-Cycle THz Pulses, Phys. Rev. Lett. **112**, 143006 (2014).
[32] C. Raman, C. W. S. Conover, C. I. Sukenik, and P. H. Bucksbaum, Ionization of Rydberg Wave Packets by Subpicosecond, Half-Cycle Electromagnetic Pulses, Phys. Rev. Lett. **76**, 2436 (1996).
[33] R. R. Jones, Creating and Probing Electronic Wave Packets Using Half-Cycle Pulses, Phys. Rev. Lett. **76**, 3927 (1996).
[34] T. J. Bensky, M. B. Campbell, and R. R. Jones, Half-Cycle Pulse Assisted Electron-Ion Recombination, Phys. Rev. Lett. **81**, 3112 (1998).
[35] M. Ranke, S. Walther, T. Gebert, A. Dimitriou, M. Sumfleth, M. J. Prandolini, M. Wieland, M. Drescher, and U. Frühling, Velocity map imaging spectrometer with an electric-field-matched gas capillary, Meas. Sci. Technol. **32**, 095901 (2021).
[36] A. T. J. B. Eppink and D. H. Parker, Velocity map imaging of ions and electrons using electrostatic lenses: Application in photoelectron and photofragment ion imaging of molecular oxygen, Rev. Sci. Instrum. **68**, 3477 (1997).
[37] M. Drescher, M. Hentschel, R. Kienberger, G. Tempea, C. Spielmann, G. A. Reider, P. B. Corkum, and F. Krausz, X-ray pulses approaching the attosecond frontier, Science **291**, 1923 (2001).
[38] J. Itatani, F. Quéré, G. L. Yudin, M. Yu. Ivanov, F. Krausz, and P. B. Corkum, Attosecond Streak Camera, Phys. Rev. Lett. **88**, 173903 (2002).
[39] E. Goulielmakis, M. Uiberacker, R. Kienberger, A. Baltuska, V. Yakovlev, A. Scrinzi, Th. Westerwalbesloh, U. Kleineberg, U. Heinzmann, M. Drescher, and F. Krausz, Direct measurement of light waves, Science **305**, 1267 (2004).
[40] M.-H. Xu, L.-Y. Peng, Z. Zhang, Q. Gong, X.-M. Tong, E. A. Pronin, and A. F. Starace, Attosecond Streaking in the Low-Energy Region as a Probe of Rescattering, Phys. Rev. Lett. **107**, 183001 (2011).
[41] L. Chen, C. Huang, X. Zhu, P. Lan, and P. Lu, Molecular photoelectron holography by an attosecond XUV pulse in a strong infrared laser field, Opt. Express **22**, 20421 (2014).
[42] A. K. Kazansky, A. V. Bozhevolnov, I. P. Sazhina, and N. M. Kabachnik, Attosecond near-threshold photoionization in a strong laser field, Phys. Rev. A **90**, 033409 (2014).
[43] J.-W. Geng, W.-H. Xiong, X.-R. Xiao, Q. Gong, and L.-Y. Peng, Steering continuum electron dynamics by low-energy attosecond streaking, Phys. Rev. A **94**, 023411 (2016).
[44] X. Yu, M. Li, M. Han, and Y. Liu, Controlling backward-scattering photoelectron holography by attosecond streaking, Phys. Rev. A **98**, 013415 (2018).
[45] J. Liang, Y. Zhou, J. Tan, M. He, Q. Ke, Y. Zhao, M. Li, W. Jiang, and P. Lu, Low-energy photoelectron interference structure in attosecond streaking, Opt. Express **27**, 37736 (2019).
[46] P. M. Paul, E. S. Toma, P. Breger, G. Mullot, F. Augé, Ph. Balcou, H. G. Muller, and P. Agostini, Observation of a train of attosecond pulses from high harmonic generation, Science **292**, 1689 (2001).
[47] P. Johnsson, R. López-Martens, S. Kazamias, J. Mauritsson, C. Valentin, T. Remetter, K. Varjú, M. B. Gaarde, Y. Mairesse, H. Wabnitz, P. Salières, Ph. Balcou, K. J. Schafer, and A. L'Huillier, Attosecond Electron Wave Packet Dynamics in Strong Laser Fields, Phys. Rev. Lett. **95**, 013001 (2005).
[48] P. Johnsson, J. Mauritsson, T. Remetter, A. L'Huillier, and K. J. Schafer, Attosecond Control of Ionization by Wave-Packet Interference, Phys. Rev. Lett. **99**, 233001 (2007).
[49] P. Ranitovic, X. M. Tong, B. Gramkow, S. De, B. DePaola, K. P. Singh, W. Cao, M. Magrakvelidze, D. Ray, I. Bocharova, H. Mashiko, A. Sandhu, E. Gagnon, M. M. Murnane, H. C. Kapteyn, I. Litvinyuk, and C. L. Cocke, IR-assisted ionization of helium by attosecond extreme ultraviolet radiation, New J. Phys. **12**, 013008 (2010).
[50] J. Mauritsson *et al.*, Attosecond Electron Spectroscopy Using a Novel Interferometric Pump-Probe Technique, Phys. Rev. Lett. **105**, 053001 (2010).
[51] J. Mauritsson, P. Johnsson, E. Mansten, M. Swoboda, T. Ruchon, A. L'Huillier, and K. J. Schafer, Coherent Electron Scattering Captured by an Attosecond Quantum Stroboscope, Phys. Rev. Lett. **100**, 073003 (2008).
[52] G. Gademann, F. Kelkensberg, W. K. Siu, P. Johnsson, M. B. Gaarde, K. J. Schafer, and M. J. J. Vrakking, Attosecond control of electron–ion recollision in high harmonic generation, New J. Phys. **13**, 033002 (2011).
[53] D. Azoury, M. Krüger, G. Orenstein, H. R. Larsson, S. Bauch, B. D. Bruner, and N. Dudovich, Self-probing spectroscopy of XUV photo-ionization dynamics in atoms subjected to a strong-field environment, Nat. Commun. **8**, 1453 (2017).
[54] B. B. Hu, X. C. Zhang, D. H. Auston, and P. R. Smith, Free space radiation from electro optic crystals, Appl. Phys. Lett. **56**, 506 (1990).

[55] J. Hebling, G. Almási, I. Z. Kozma, and J. Kuhl, Velocity matching by pulse front tilting for large-area THz-pulse generation, Opt. Express **10**, 1161 (2002).
[56] M. Ranke, Investigation of low-energy photoelectron dynamics accelerated in terahertz light fields using a novel velocity-map-imaging spectrometer, Ph.D. thesis, Universität Hamburg, 2019.
[57] A. E. S. Green, D. L. Sellin, and A. S. Zachor, Analytic independent-particle model for atoms, Phys. Rev. **184**, 1 (1969).
[58] Q. Zhang, P. Lan, and P. Lu, Empirical formula for over-barrier strong-field ionization, Phys. Rev. A **90**, 043410 (2014).
[59] We use the Green-Sellin-Zachor potential of [58] with the modified parameter $H = 6.8163$.
[60] X.-M. Tong and S.-I. Chu, Theoretical study of multiple high-order harmonic generation by intense ultrashort pulsed laser fields: A new generalized pseudospectral time-dependent method, Chem. Phys. **217**, 119 (1997).
[61] M. Murakami, O. Korobkin, and M. Horbatsch, High-harmonic generation from hydrogen atoms driven by two-color mutually orthogonal laser fields, Phys. Rev. A **88**, 063419 (2013).
[62] R. R. Freeman, P. H. Bucksbaum, H. Milchberg, S. Darack, D. Schumacher, and M. E. Geusic, Above-Threshold Ionization with Subpicosecond Laser Pulses, Phys. Rev. Lett. **59**, 1092 (1987).
[63] J. Dura, N. Camus, A. Thai, A. Britz, M. Hemmer, M. Baudisch, A. Senftleben, C. D. Schröter, J. Ullrich, R. Moshammer, and J. Biegert, Ionization with low-frequency fields in the tunneling regime, Sci. Rep. **3**, 2675 (2013).
[64] B. Wolter, C. Lemell, M. Baudisch, M. G. Pullen, X.-M. Tong, M. Hemmer, A. Senftleben, C. D. Schröter, J. Ullrich, R. Moshammer, J. Biegert, and J. Burgdörfer, Formation of very-low-energy states crossing the ionization threshold of argon atoms in strong mid-infrared fields, Phys. Rev. A **90**, 063424 (2014).
[65] S. Larimian, S. Erattupuzha, C. Lemell, S. Yoshida, S. Nagele, R. Maurer, A. Baltuška, J. Burgdörfer, M. Kitzler, and X. Xie, Coincidence spectroscopy of high-lying Rydberg states produced in strong laser fields, Phys. Rev. A **94**, 033401 (2016).
[66] U. Frühling, M. Wieland, M. Gensch, T. Gebert, B. Schütte, M. Krikunova, R. Kalms, F. Budzyn, O. Grimm, J. Rossbach, E. Plönjes, and M. Drescher, Single-shot terahertz-field-driven X-ray streak camera, Nat. Photonics **3**, 523 (2009).
[67] B. Schütte, U. Frühling, M. Wieland, A. Azima, and M. Drescher, Electron wave packet sampling with laser-generated extreme ultraviolet and terahertz fields, Opt. Express **19**, 18833 (2011).
[68] See Supplemental Material at http://link.aps.org/supplemental/10.1103/PhysRevLett.129.213202 for an animated presentation of the 2D projections and a discussion of the dynamics of zero-energy electrons.
[69] X.-B. Bian, Y. Huismans, O. Smirnova, K.-J. Yuan, M. J. J. Vrakking, and A. D. Bandrauk, Subcycle interference dynamics of time-resolved photoelectron holography with midinfrared laser pulses, Phys. Rev. A **84**, 043420 (2011).
[70] X. Wang and F. Robicheaux, Ionization from Rydberg atoms and wave packets by scaled terahertz single-cycle pulses, Phys. Rev. A **99**, 033418 (2019).
[71] C. Nicole, I. Sluimer, F. Rosca-Pruna, M. Warntjes, M. Vrakking, C. Bordas, F. Texier, and F. Robicheaux, Slow Photoelectron Imaging, Phys. Rev. Lett. **85**, 4024 (2000).
[72] C. Bordas, Classical motion of a photoelectron interacting with its ionic core: Slow photoelectron imaging, Phys. Rev. A **58**, 400 (1998).
[73] E. Diesen, U. Saalmann, M. Richter, M. Kunitski, R. Dörner, and J. M. Rost, Dynamical Characteristics of Rydberg Electrons Released by a Weak Electric Field, Phys. Rev. Lett. **116**, 143006 (2016).
[74] S. Larimian, C. Lemell, V. Stummer, J.-W. Geng, S. Roither, D. Kartashov, L. Zhang, M.-X. Wang, Q. Gong, L.-Y. Peng, S. Yoshida, J. Burgdörfer, A. Baltuška, M. Kitzler, and X. Xie, Localizing high-lying Rydberg wave packets with two-color laser fields, Phys. Rev. A **96**, 021403(R) (2017).
[75] P. Ge and Y. Liu, Control of the yield of surviving Rydberg atoms in strong-field ionization with two-color laser fields, J. Phys. B **50**, 125001 (2017).
[76] A. von Veltheim, B. Manschwetus, W. Quan, B. Borchers, G. Steinmeyer, H. Rottke, and W. Sandner, Frustrated Tunnel Ionization of Noble Gas Dimers with Rydberg-Electron Shakeoff by Electron Charge Oscillation, Phys. Rev. Lett. **110**, 023001 (2013).
[77] X. Zhang, R. R. Jones, and F. Robicheaux, Time-Dependent Electron Interactions in Double Rydberg Wave Packets, Phys. Rev. Lett. **110**, 023002 (2013).

Correction: The name of the institution in the fourth affiliation contained an error and has been fixed.